

# Photoinduced Electron Transfer in Os(terpyridine)-biphenylene-(bi)pyridinium Assemblies

Jérôme Fortage,<sup>†</sup> Fausto Puntoriero,<sup>\*,‡</sup> Fabien Tuyères,<sup>†</sup> Grégory Dupeyre,<sup>†</sup> Antonino Arrigo,<sup>‡</sup> Ilaria Ciofini,<sup>§</sup> Philippe P. Lainé,<sup>\*,†</sup> and Sebastiano Campagna<sup>\*,‡</sup>

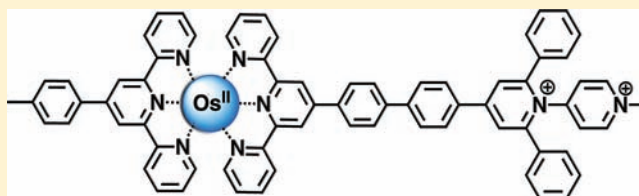
<sup>†</sup>Université Paris Diderot, Sorbonne Paris Cité, ITODYS, UMR 7086 CNRS, 15 rue Jean-Antoine de Baïf, 75013 Paris, France

<sup>‡</sup>Dipartimento di Chimica Inorganica, Chimica Analitica e Chimica Fisica and Centro Interuniversitario per la Conversione Chimica dell'Energia Solare (SolarChem-sezione di Messina), Università di Messina, Via Stagno d'Alcontres 31, I-98166 Messina, Italy

<sup>§</sup>École Nationale Supérieure de Chimie de Paris—Chimie ParisTech, LECIME, UMR 7575 CNRS, 11 rue Pierre et Marie Curie, 75005 Paris, France

## S Supporting Information

**ABSTRACT:** A series of linearly arranged donor-spacer-acceptor (D-S-A) systems 1–3, has been prepared and characterized. These dyads combine an Os(II)bis(terpyridine) unit as the photoactivable electron donor (D), a biphenylene (2) or phenylene-xylylene (3) fragment as the spacer (S), and a *N*-aryl-2,6-diphenylpyridinium electrophore (with aryl = 4-pyridyl or 4-pyridylum in 1 or 2/3, respectively) as the acceptor (A). Their absorption spectra, redox behavior, and luminescence properties (both at 77 K in rigid matrix and at 298 K in fluid solution) have been studied. The electronic structure and spectroscopic properties of a representative compound of the series (i.e., 2) have also been investigated at the theoretical level, performing Density Functional Theory (DFT)-based calculations. Time-dependent transient absorption spectra of 1–3 have also been recorded at room temperature. The results indicate that efficient photoinduced oxidative electron transfer takes place in the D-S-A systems at room temperature in fluid solution, for which rate constants (in the range  $4 \times 10^8$ – $2 \times 10^{10} \text{ s}^{-1}$ ) depend on the driving force of the process and the spacer nature. In all the D-S-A systems, charge recombination is faster than photoinduced charge separation, in spite of the relatively large energy of the  $\text{D}^+\text{-S-A}^-$  charge-separated states (between 1.47 and 1.78 eV for the various species), which would suggest that the charge recombination occurs in the Marcus inverted region. Considerations based on superexchange mechanism suggest that the reason for the fast charge recombination is the presence of a virtual  $\text{D-S}^+\text{-A}^-$  state at low energy—because of the involvement of the easily oxidizable biphenylene spacer—which is beneficial for charge recombination via superexchange but unsuitable for photoinduced charge separation. To further support the above statement, we prepared a fourth D-S-A species, 4, analogous to 2 but with a (hardly oxidizable) single phenylene fragment serving as the spacer. For such a species, charge recombination (about  $3 \times 10^{10} \text{ s}^{-1}$ ) is slower than photoinduced charge separation (about  $1 \times 10^{11} \text{ s}^{-1}$ ), thereby confirming our suggestions.



## 1. INTRODUCTION

Long-range photoinduced electron transfer plays a key role in both natural and artificial systems.<sup>1</sup> Examples are natural photosynthesis as well as synthetic assemblies for solar energy conversion and information technologies.<sup>1,2</sup> Among the synthetic assemblies, linearly arranged donor-spacer-acceptor species (D-S-A, where each subunit preserves its own electronic and redox properties, to a first approximation) are particularly attractive, as they allow control over several parameters including donor–acceptor distance, so opening the way, when a series of homogeneous species is available, to infer useful detailed information on the effects of energetics and spacer properties on the photoinduced electron transfer process.<sup>1–4</sup>

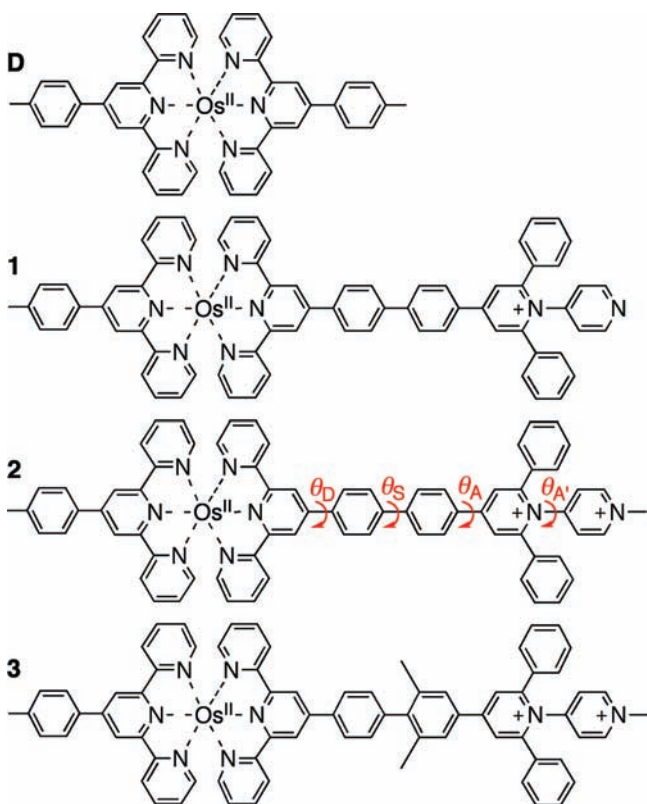
We have recently prepared a large series of (bi)pyridinium-based species, referred to as expanded pyridiniums, and studied their photophysical and redox properties.<sup>5,6</sup> Beside their

interesting luminescence properties, these species show appealing structural and electrochemical features (including reversible reduction processes at relatively mild potentials), which make them good candidates to play the role of acceptors (A) in suitably designed D-S-A systems. We have now connected some of such expanded pyridinium species to Os(II) bis-terpyridine chromophores, to prepare a series of linearly arranged D-S-A assemblies. Here are presented the photophysical properties of a first set of such compounds (dyads 1–3 in Chart 1), with a special emphasis on their ability to undergo directional photoinduced electron transfer processes. Synthesis and characterization of these dyads are given in the Supporting Information. In 1–3, an Os(II)-based inorganic subunit<sup>7</sup> plays the role of the light-triggered electron

Received: February 9, 2012

Published: April 23, 2012

**Chart 1. Structural Formulae and Nomenclature of the D-S-A Assemblies (1–3) Synthesized and Studied along with That of Reference (D)<sup>a</sup>**



<sup>a</sup> Total charges are omitted. Counterions are  $\text{PF}_6^-$  anion.

donor, the biphenylene moiety or its tilted phenylene-xylylene analogue is the semirigid spacer (which structure guarantees a fixed donor–acceptor distance within the series), and the *N*-pyridyl-2,6-diphenylpyridinium subunit or its quaternized form (*head-to-tail*-bipyridinium) is the acceptor component (*head-to-tail*-bipyridinium is the isomer of archetypal *tail-to-tail*-bipyridinium electron acceptor, that is methyl viologen). Interestingly, the *head-to-tail* layout of the two heterocycles allows to connect A while maintaining both the overall semirigidity and the desirable rod-like shape of the D-S-A assembly. Compounds 1 and 2 differ from one another by the driving force of the intercomponent electron transfer process, whereas 2 and 3 differ by the conformation of their biphenylene spacer, represented by torsional angles  $\theta_S$  (see Chart 1).

A combined theoretical and experimental approach allowed us to propose a rationalization of the results concerning the lifetime of the charge-separated states, so highlighting somewhat underestimated issues of general importance which should be taken into account for the design of D-S-A species aimed at

generating long-lived charge-separated states. To further support our analysis we prepared another D-S-A system, compound 4, containing a shorter spacer (compound 4 is identical to 2, but the biphenylene spacer is replaced by a single phenylene spacer), and studied its photophysical properties.

## 2. RESULTS AND DISCUSSION

**2.1. Redox Behavior and Electronic Absorption Spectra.** Table 1 collects the oxidation and first reduction potentials (acetonitrile solution, MeCN) of 1–3 (the D-S-A species) and of the reference compound D. The first reduction potentials measured for 1–3 are straightforwardly assigned to pyridinium-centered processes,<sup>6</sup> as they are significantly less negative than that observed for D, which is phtpy-centered by nature (phtpy = 4'-phenyl-2,2':6',2''-terpyridine).<sup>7</sup> Interestingly, the reduction potentials of the free acceptors<sup>6</sup> (for free acceptors we consider the S-A species, missing the  $\{\text{Os}(\text{tpy})_2\}^{2+}$  unit; tpy = 2,2':6',2''-terpyridine), are almost identical to those of the corresponding D-S-A species (see Table 1). This indicates that the electronic coupling between D and A in the D-S-A assemblies is roughly negligible at the ground state, as further confirmed by comparison between absorption spectra of D and 1–3 (Figure 1): the metal-to-ligand charge-transfer

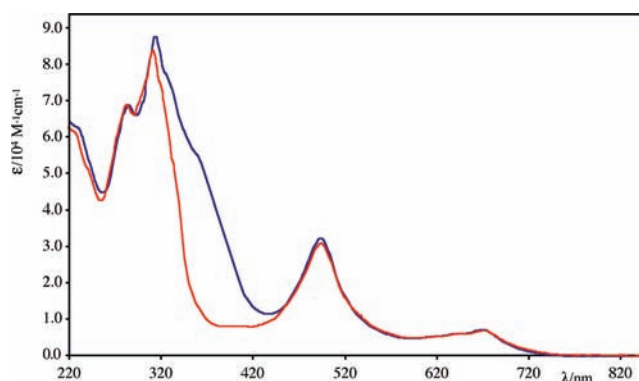


**Figure 1.** Absorption spectra of D (red line) and of 2 (blue line) in MeCN solution at 298 K.

(MLCT) bands at wavelengths longer than 430 nm are indeed almost identical for all the compounds, showing that the Os(II)-based chromophore is essentially unperturbed by the various acceptor units. The only significant difference in the absorption spectra of 1–3 compared to D is observed in the UV region, and is ascribed to (bi)pyridinium-centered electronic transitions. Taken together, the redox and electronic absorption properties indicate that 1–3 can be regarded as supramolecular species, supporting the weak coupling limit intrinsic to the D-S-A notation.<sup>8</sup>

**Table 1. Redox and Electronic Absorption Data along with Assignments.<sup>a</sup>**

species	redox data, V vs SCE		$\lambda_{\text{max}}$ nm ( $\epsilon$ , $10^4 \text{ M}^{-1} \text{ cm}^{-1}$ )		
	$E_{1/2}^{\text{ox}}$	$E_{1/2}^{\text{red}}$	ligand-centered (LC)	<sup>1</sup> MLCT	<sup>3</sup> MLCT
1	+0.89	−0.89 (−0.91) <sup>b</sup>	317 (8.85)	493 (3.10)	676 (0.72)
2	+0.89	−0.58 (−0.58) <sup>b</sup>	317 (8.98)	492 (3.05)	676 (0.71)
3	+0.89	−0.61 (−0.60) <sup>b</sup>	317 (8.91)	494 (3.15)	675 (0.74)
D	+0.88	−1.22	314 (8.64)	490 (3.01)	668 (0.77)

<sup>a</sup>MeCN solutions. <sup>b</sup>The value in brackets is the reduction potential for the corresponding S–A species, taken from ref 6.

To feed the discussion about the electronic structure and absorption properties of D-S-A dyads (the term dyad is here used to specify the presence of two *active* subunits, the donor and acceptor, whereas the spacer subunit has mainly a structural function, at least in a first approximation), the case study of dyad **2** was specifically investigated at the theoretical level, by performing density functional theory (DFT)-based calculations (see Experimental Section for technical details). As regards the structural level, the geometry of the molecule was fully optimized (using the global hybrid functional PBE0) taking into account effects of bulk solvent (MeCN) by the means of the polarizable continuum model (PCM). It has been recently proven that this level of theory yields a good description of both the electronic and geometrical features of transition metal complexes,<sup>9</sup> including the case of the present type of dyads.<sup>10</sup> The main computed structural parameters are reported in Supporting Information, Table S1. As expected, the first coordination sphere of osmium(II) is rather symmetric and only a small (0.004 Å) contraction in the Os–N distance for the tpy carrying the acceptor can be noted. This finding further substantiates the above inference that D and A subsystems are rather decoupled at the ground state. Nonetheless, from the structural point of view, the values of torsion angles ( $\theta$ ; Chart 1) computed between the different aryl subunits along the main molecular axis of D-S-A reveal that an intercomponent electronic coupling should, however, be present. Indeed, beside the rather small interannular angle within the biphenylene spacer ( $\theta_s = 27^\circ$ ), dihedral angles between the tpy and the biphenylene linker ( $\theta_D$ ) and between the spacer and the (bi)pyridinium-based acceptor ( $\theta_A$ ) are both quite small: roughly  $27^\circ$  and  $20^\circ$ , respectively.

As regards electronic features, vertical excitations energies were computed at the time-dependent DFT (TD-DFT) level using the range-separated CAM-B3LYP functional. This functional was selected to ensure the absence of artifacts in the reproduction of long-range charge-transfer (CT) excitations, which can be present when using global hybrid functionals (including PBE0). In spite of the known systematic, and slight, overestimation of absolute transitions energies computed at CAM-B3LYP level,<sup>11</sup> there is a good agreement between experimental and calculated data, as shown in Figure 2 for dyad **2**.

The computed vertical transitions and associated oscillator strengths ( $f$ ) are collected in Table 2 together with their assignments in terms of one-electron excitations (only transitions with significant intensity ( $f > 0.04$  au) at  $\lambda > 300$  nm are reported; see the Supporting Information, Table S2 for full data).<sup>12</sup> Molecular orbitals (MOs) involved in these transitions are shown in Figure 3.

From the computed data, three main absorptions bands are predicted. The lower energy transition, found at 459 nm, has a dominant MLCT character, with a non-negligible contribution from the (L+2) orbital involving the acceptor A moiety. Three electronic transitions (computed at 399, 396, and 391 nm) contribute to the second absorption band. All these transitions are of MLCT type and the involved orbitals are all mainly centered on the D core. Finally, the dominant absorption band is associated to a very intense transition computed at 359 nm, corresponding to CT excitations from essentially the biphenylene spacer (S) to the *head-to-tail*-bipyridinium acceptor (A).

Therefore, the overall picture we get from these calculations can be summarized as follows: the bands at the red edge

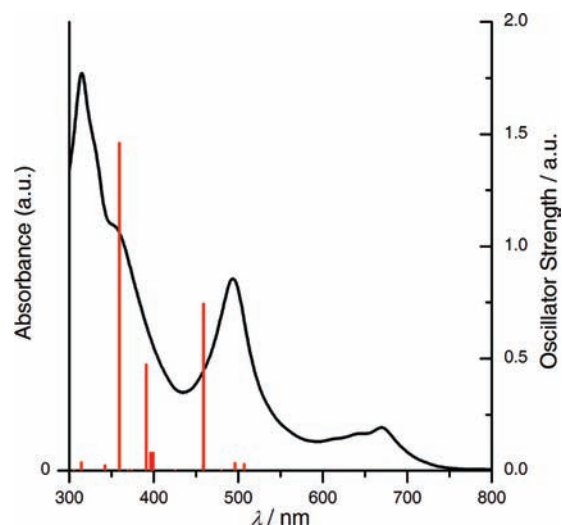


**Figure 2.** Superimposed experimental absorption spectrum of **2** (MeCN solution) and corresponding calculated electronic transitions (spin-forbidden transitions related to  $^3\text{MLCT}$  features are not represented; see text).

**Table 2.** Computed (CAM-B3LYP/PCM) Transitions (Wavelength,  $\lambda$ , in nm) of Lowest Energy and Associated Oscillator Strengths ( $f$ , au) Together with Their Orbital Contributions<sup>a</sup>

$\lambda$	$f$	orbital contribution
459	0.743	(H-2)-(L+3); (H-1)-(L+2)
399	0.079	(H-1)-(L+4); (H-1)-(L+5)
396	0.079	(H-2)-(L+4); (H-2)-(L+5)
391	0.472	H-(L+4)
359	1.460	(H-3)-L; (H-3)-(L+1); (H-1)-L

<sup>a</sup>H: HOMO and L: LUMO.

(computed at 459 nm and around 395 nm) are roughly “classical” MLCT bands, corresponding to the formation of the  $^*\text{D-S-A}$  state (although for the lower energy one, some  $\text{D}^+\text{-S-A}^-$  character is present). In particular, the calculated 459 nm band corresponds to the experimental absorption band peaking at about 492 nm, and the calculated contribution at 395 nm probably corresponds to absorption features at about 450 nm in the experimental spectrum, largely obscured by more intense bands (see Figure 2). The most intense and higher-energy calculated band at 359 nm is associated with a  $\text{D-S}^+\text{-A}^-$  state, and is reflected in the experimental intense absorption around 360 nm.<sup>14</sup>

**2.2. Luminescence Properties and Photoinduced Electron Transfer Processes.** The luminescence properties of **1–3** at 77 K in a butyronitrile rigid matrix are perfectly identical to one another and to those of **D** (see Table 3, which collects photophysical data of all compounds, along with kinetic and thermodynamic data for electron transfer processes). Emission is clearly due to a triplet MLCT state.<sup>15</sup> At room temperature in fluid MeCN solution, however, the MLCT emission of **D** is largely quenched in **1** and **3** (the MLCT emission lifetime, 240 ns for **D**, is 11.3 and 2.2 ns for **1** and **3**, respectively) and is totally quenched in **2** (Table 3).

In weakly coupled  $^*\text{D-S-A}$  species, intercomponent, photoinduced electron and/or energy transfer processes have to be considered as decay pathways. However, the triplet states of the S-A subunits of **1–3** lie at higher energy than 600 nm,<sup>6</sup> so the

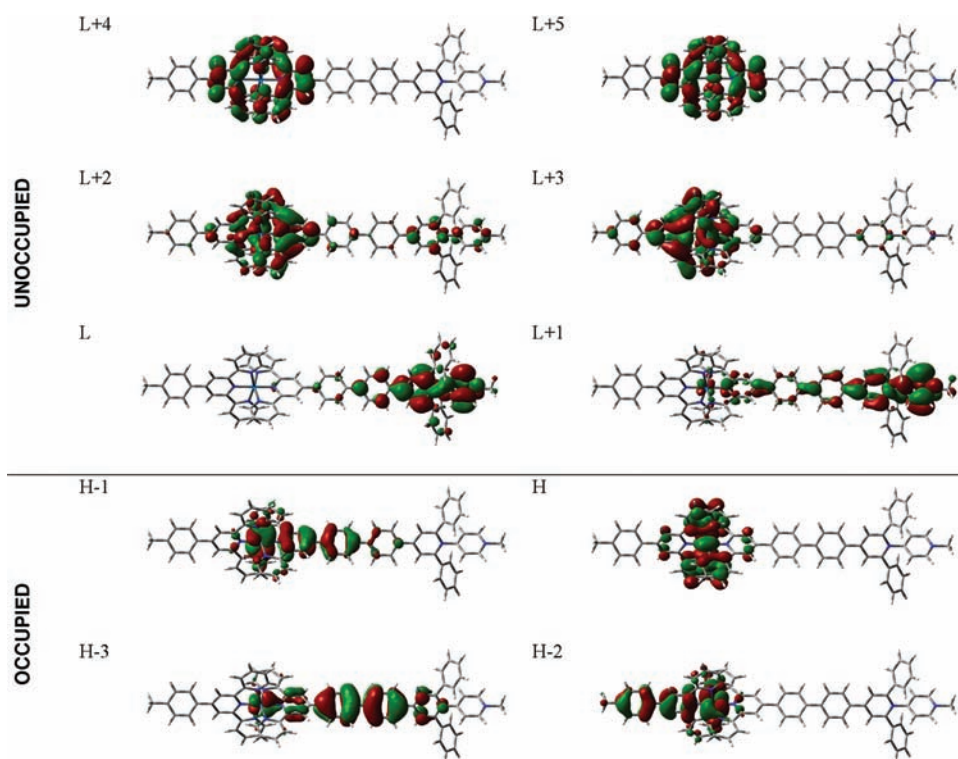


**Figure 3.** Isocontour plots (isocontour value 0.02 au) of MOs involved in significant low-energy transitions ( $\lambda > 300$  nm; Table 2); H: HOMO; L: LUMO.

**Table 3. Luminescence Data along with Thermodynamic and Kinetic Parameters for the Photoinduced Electron Transfer (PET) Processes<sup>a</sup>**

compound	luminescence, 77 K <sup>b</sup>		luminescence, 298 K			PET parameters	
	$\lambda_{\text{max}}$ , nm	$\tau$ , ns	$\lambda_{\text{max}}$ , nm	$\tau$ , ns	$\Phi$	$(\Delta G^0)^c$	$k_{\text{et}}$ , s <sup>-1</sup>
1	723	2800	745	11.3 <sup>d</sup>	$2.3 \times 10^{-3}$	+0.06	$2.6 \times 10^{9e}$
2	723	2800		no emission		-0.25	$1.5 \times 10^{10}$
3	723	2800	740	2.2	$1.3 \times 10^{-3}$	-0.22	$4.5 \times 10^8$
D	723	2880	740	240	0.02		

<sup>a</sup>Data collected at 298 K in MeCN solution, unless otherwise indicated. <sup>b</sup>Data in butyronitrile (BuCN) rigid matrix. <sup>c</sup>Driving force calculated as described in the text. <sup>d</sup>This emission lifetime is assigned to an equilibrated excited state (see text). <sup>e</sup>This figure represents an upper limit, as it is the equilibration rate constant between the initially prepared <sup>3</sup>MLCT and the charge-separated state (see text).

energy transfer route from the MLCT state to the S-A triplet states can be ruled out. The driving force  $\Delta G^0$  for photoinduced oxidative electron transfer at room temperature, leading from <sup>\*</sup>D-S-A to D<sup>+</sup>-S-A<sup>-</sup>, can be approximated on the basis of redox and spectroscopic data, assuming the validity of the Koopman theorem, according to eq 1.

$$\Delta G^0 = (*E_{\text{ox}} - E_{\text{red}}) + W \quad (1)$$

$$*E_{\text{ox}} = E_{\text{ox}} - E^{0-0} \quad (2)$$

In eq 1,  $*E_{\text{ox}}$  is the oxidation potential of the excited state of the donor chromophore (expressed, as all the other similar terms in eqs 1 and 2, as one-electron energies, in eV), in its turn approximated from eq 2, where  $E_{\text{ox}}$  is the ground state oxidation potential of the donor and  $E^{0-0}$  is the excited state energy, assumed as the emission maximum at 77 K. The term  $E_{\text{red}}$  is the reduction potential of the acceptor, corresponding to the first reduction potential of the D-S-A system. The term  $W$ , called the work term, is the difference between Coulombic stabilization energies of reactants and products; its effect is to

(slightly) reduce the driving force; however, it is often neglected. Equations 1 and 2 yield  $\Delta G^0$  values of +0.06 eV for **1**, -0.25 eV for **2**, and -0.22 eV for **3** (data reported in Table 3), indicating that the <sup>3</sup>MLCT excited state and the charge-separated D<sup>+</sup>-S-A<sup>-</sup> state are roughly iso-energetic in **1** while the electron transfer is slightly exergonic for **2** and **3**.<sup>16</sup> So, oxidative electron transfer is thermodynamically feasible as MLCT decay in **1**–**3** at room temperature in fluid solution, although with modest driving forces. Because of this modest driving force, such a decay process is anyway expected to be impeded at 77 K in rigid matrix, because of the destabilization of the charge-separated state and/or of nuclear barriers,<sup>17</sup> so justifying the luminescence data of **1**–**3** at low temperature.

The time-resolved transient absorption spectrum of **1** (excitation wavelength, 400 nm), obtained by using a pump-probe equipment, is shown in Figure 4: it exhibits two bleachings peaking at about 490 and 670 nm, corresponding to singlet and triplet MLCT absorption bands, and transient absorptions in the region 540–640 nm and at wavelength longer than 700 nm, assigned to the absorption of reduced terpyridine ligand, partially overlapped with the bleaching of

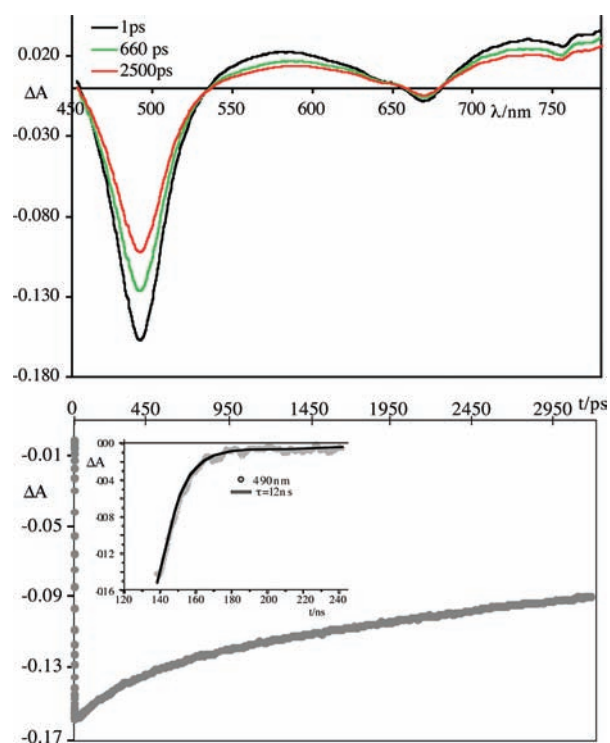


**Figure 4.** Transient absorption spectra (top; delay times are indicated in the panel) and decay (bottom) of **1** in MeCN solution (excitation wavelength, 400 nm). The absorption recovery trace in the shorter time scale is fitted by two exponentials (see text). The longer-lived component is visualized in the inset, recorded in the nanosecond time range.

the MLCT spin-forbidden absorption. This transient spectrum is identical to that of **D** (shown in the Supporting Information). However, whereas the transient spectrum of **D** decays monoexponentially (excluding some rearrangements in the femtosecond time scale, not investigated here) on a nanosecond time scale, in agreement with luminescence lifetime data, the transient spectrum of **1** decays biexponentially to the ground state with lifetimes of 380 ps (minor component) and 12 ns (the dominant component); this second decay was monitored using a nanosecond flash photolysis apparatus). We assign the faster lifetime to the equilibration process between the closely lying  $^3\text{MLCT}$  and charge-separated states, and the slower decay lifetime, which is in good agreement with the emission lifetime measured by single-photon-counting luminescence apparatus, to the decay of the equilibrated state. Equilibration between excited states is not unusual for MLCT triplet states of metal complexes,<sup>18</sup> including Os(II) polypyridine compounds.<sup>7,10a,19</sup> Since during equilibration the relative populations of the two different excited states (MLCT and charge-separated) change, one would expect a change in the transient spectra shape. However, no sizable spectral evolution associated with the equilibration time is present in the decay of the transient spectrum. This is not surprising because, according to the Boltzmann distribution, the population of the equilibrated state largely involves (with at least a 90% contribution) the MLCT state and therefore the transient spectrum of the equilibrated state is not significantly different from that of the initially formed MLCT state.

It can be noted that excitation at 400 nm (the exciting wavelength used in the pump–probe experiments) in **1–3** also directly excites the S-A unit (see Figure 1). However, this

excitation leads with high efficiency to the population of the  $^3\text{MLCT}$  (most likely via the lowest-lying  $^1\text{MLCT}$  and successive intersystem crossing), as the emission quantum yields of **1** and **3** are independent from excitation wavelength in the studied range (380–620 nm). Compound **2** is not emissive, so the constancy of emission quantum yield cannot be employed to infer information on the fate of the direct excitation of the S-A unit in **2**; anyway there is no valid reason to believe that **2** behaves differently from **1** and **3**.

The time-resolved transient absorption spectra of **2** and **3** are shown in Figure 5. In both cases, the decay of the transient

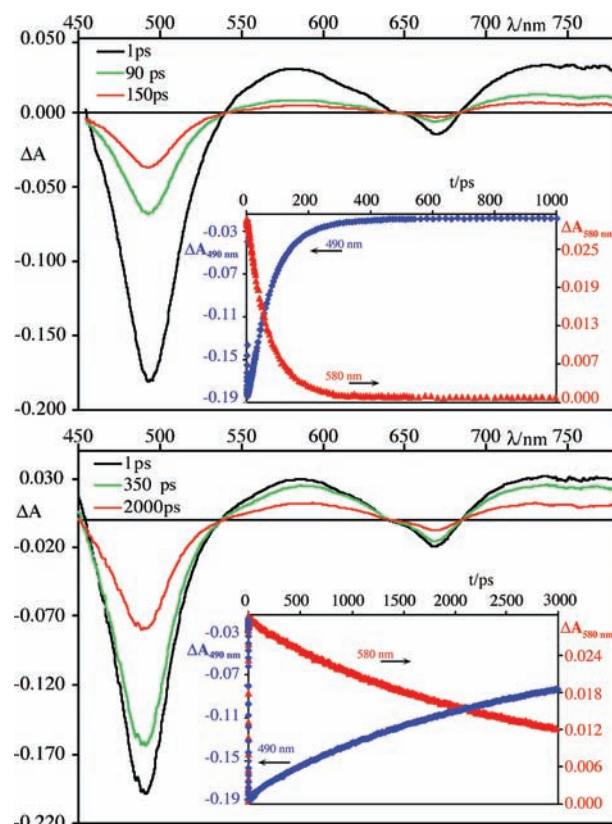


**Figure 5.** Transient spectra and decays ( $\lambda = 490$  and 580 nm) of **2** (top panel) and **3** (bottom panel) in MeCN solution. Excitation wavelength, 400 nm.

absorption (calculated at two different wavelengths for each species, corresponding to bleaching recovery at 490 nm and transient decay at 580 nm) is monoexponential, yielding 67 ps and 2.2 ns, corresponding to photoinduced oxidative electron transfer rate constants of  $1.5 \times 10^{10} \text{ s}^{-1}$  and  $4.5 \times 10^8 \text{ s}^{-1}$  for **2** and **3**, respectively. As the driving forces for photoinduced electron transfer in **2** and **3** are very close (see Table 3), their rather different rate constants are attributed to the nature of the spacer. In weakly coupled D-S-A species, superexchange-mediated photoinduced oxidative electron transfer takes advantage of virtual states involving the lowest unoccupied molecular orbital (LUMO) spacer orbitals (here we assume that the effective superexchange pathway for photoinduced electron transfer in **1–3** is electron transfer, see also below).<sup>20</sup> Given that (i) the geometrical decoupling due to the presence of substituents in the spacer structure of **3** ( $\theta_S$  approaches  $90^\circ$ ) destabilizes LUMO spacer orbitals in comparison to the corresponding orbitals of **2**, and (ii) the superexchange-

mediated electronic coupling between excited donor and acceptor is inversely proportional to the energy gap between the highest-energy occupied orbital of the excited donor and the lowest-lying vacant orbitals centered on the spacer,<sup>20</sup> the presence of methyl substituents on the biphenylene spacer of **3** (i.e., xylylene fragment) results in a significantly reduced electronic coupling for photoinduced electron transfer, and hence the slower rate constant derived for the oxidative electron transfer for **3**.

Noteworthy, for **2** and **3** the transient spectra recorded at different delay times (Figure 5) show “isobestic” points at  $\Delta\text{Abs} = 0$ , which are held for the whole decay process. The isobestic points are almost identical for both compounds, and are at about 540, 645, and 690 nm. This confirms that only two states are present during the decay processes, the initially formed <sup>3</sup>MLCT and the ground state.

Comparison between electron transfer rate constants of **1** and **2**, which share the same spacer, highlights the effect of the driving force: the upper limit for photoinduced electron transfer in **1** is the equilibration rate constant,  $2.6 \times 10^9 \text{ s}^{-1}$ , about 1 order of magnitude slower than the electron transfer rate constant in **2**, which experiences a driving force more favorable by 0.31 eV.<sup>21</sup>

The above-mentioned results show that the D-S-A species **1–3** are instrumental to highlight the effect of driving force and spacer conformation on photoinduced electron transfer. However, probably the most striking result of the present work is the absence of a long-lived charge-separated state. In fact, in all cases the initially formed<sup>22,23</sup> transient absorption spectra decay to the ground state spectra without any spectral evolution, indicating that back electron transfer (i.e., charge recombination) is faster than forward photoinduced electron transfer (charge separation). This could appear surprising, as the driving force for charge recombination (the process leading from  $\text{D}^+\text{-S-A}^-$  to  $\text{D-S-A}$ ) is relatively large, about  $-1.78 \text{ eV}$  for **1**,  $-1.47 \text{ eV}$  for **2**, and  $-1.50 \text{ eV}$  for **3**,<sup>24</sup> much larger than driving force for photoinduced charge separation, and probably lies in the Marcus inverted region for all the compounds studied herein. Also, the donor–acceptor distance for the charge recombination processes is expected to be larger than that for charge separation: in fact, in the charge separation process, the involved orbitals are centered on the terpyridine connected to the spacer of the  $\{\text{Os}(\text{tpy})_2\}$  subunit (for D) and on the acceptor A subunits, whereas in charge recombination the relevant orbitals are the same A-centered orbitals and an Os(III)-centered one for D. Also in spite of this increased donor–acceptor distance for the back electron transfer process, which should contribute to further reduce electronic coupling for charge recombination compared to charge separation, charge recombination is faster than charge separation.

The rationale for the fast charge recombination occurring in **1–3** is revealed by a closer look at the superexchange mechanism. The rate constant for electron transfer, using a Fermi Golden Rule formalism, can be expressed as in eq 3.<sup>8</sup>

$$k_{\text{el}} = \frac{4\pi^2}{h} |H_{\text{ET}}|^2 \text{FCWD} \quad (3)$$

In eq 3,  $H_{\text{ET}}$  is the electronic coupling for the electron transfer process and FCWD is the Franck–Condon weighted density of states, which contains information concerning overlap between the vibrational wave functions of the reactants and product states, related to driving force and reorganization energy of the process. According to the McConnell super-

exchange theory,<sup>20</sup> for D-S-A systems, spacer orbitals can be involved in virtual states, so contributing to the electronic coupling between D and A subunits. Two main pathways can be effective in the superexchange mechanism for D-to-A electron transfer: (i) an electron-transfer route, implying the intervening of lowest-lying virtual MOs centered on the spacer (the virtual state assumes the form of a  $\text{D}^+\text{-S}^-\text{-A}$  state), contributing to the effective overall electronic coupling by  $H^{\text{el}}$ , and (ii) a hole-transfer pathway, which involves the highest-lying occupied MOs centered on the spacer (with participation of a  $\text{D-S}^+\text{-A}^-$  virtual state), contributing to the overall coupling by  $H^{\text{h}}$ . The spacer-mediated overall coupling  $H_{\text{ET}}$  (which is given by  $H^{\text{el}} + H^{\text{h}}$ ) inversely depends on the energy gap between the initial state and the relevant virtual states of each process.<sup>3,20,25,26</sup> Figure 6 schematizes the states involved in the

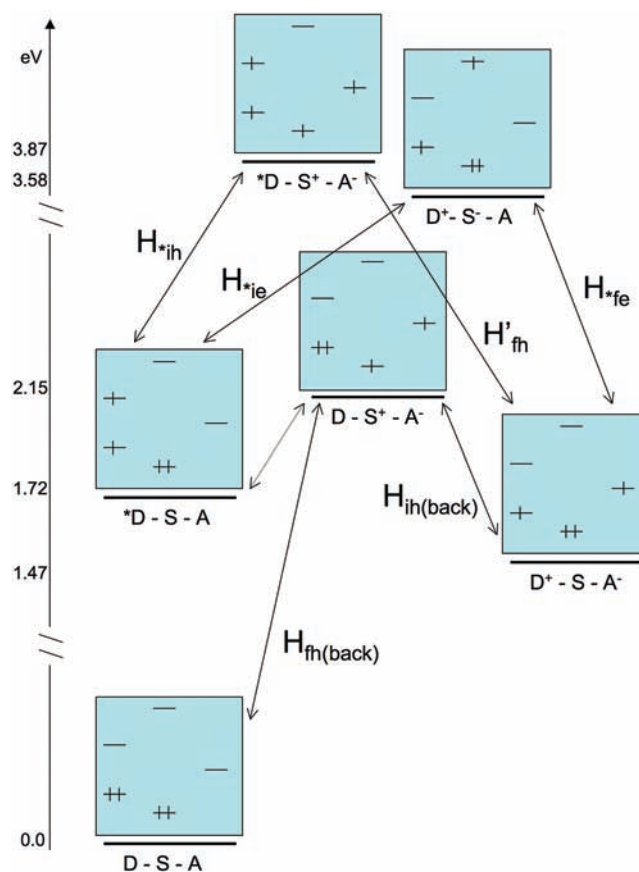


**Figure 6.** Schematization of the states involved in the superexchange-mediated electron transfer processes occurring in **2** (including pictorial representations of HOMOs and LUMOs of the D, S, and A subunits; in each single panel, the orbitals of D are represented on the left side, the orbitals of S are represented in the center column, and the orbitals of A are shown on the right). For details, see text.

superexchange mechanism for photoinduced oxidative electron transfer and charge recombination processes in **2**, here considered as a representative compound of the D-S-A supramolecular assemblies studied herein. In Figure 6, the energies of the various states are inferred from spectroscopic and redox data (Table 1), as follows.

- The emission energy of the S-A subunit of **2** (577 nm), known to originate from a charge-transfer state,<sup>6</sup> is used to estimate the energy of the virtual  $\text{*D-S}^+\text{-A}^-$  state of **2** (the energy of such a state is approximated to 3.87 eV,

that is, the sum of the excited state energy of **D** and the excited state energy of the isolated S-A species).

- The above-mentioned emission energy of the S-A subunit is also used to directly estimate the energy of the  $D^+S^-A^-$  state (2.15 eV). Note that the presence of this state at a relatively low energy fairly agrees with computed states energies (see above): in fact, this state corresponds to the one whose absorption is computed at 359 nm, not far from the computed MLCT absorption bands.
- The energy of the  $D^+S^-A$  state is roughly approximated from the difference between the potential of the first oxidation of **2** (+0.89 V, see Table 1) and the reduction potential of isolated biphenyl, which is  $-2.66$  V vs SCE in MeCN,<sup>27</sup> so yielding a value of 3.58 eV. Note that this is a rough approximation, because the biphenylene unit embedded within **2** is connected to electron withdrawing groups. Consequently, the actual  $D^+S^-A$  state is expected to lie at a slightly lower energy than that estimated above.
- The energy of the  $*D-S-A$  state is derived from the 77 K emission energy of **2**, 1.72 eV.
- The energy of the charge-separated state,  $D^+S^-A^-$  is given by eq 1, that is, 1.47 eV.

On the basis of Figure 6, the electronic matrix element for the oxidative photoinduced electron transfer  $H_{ET}$  (driving the process from the excited state  $*D-S-A$  to the charge-separated state) occurring in **2** is expressed in eq 4, whereas eq 5 shows the electronic coupling for back electron transfer ( $H_{BET}$ , driving the process from the  $D^+S^-A^-$  charge-separated state to the ground state). The expression for  $H_{BET}$  only reports the hole-transfer pathway, since the electron-transfer route for the charge recombination can be neglected in the present case because of the large energy gap between the charge-separated state  $D^+S^-A^-$  and the relevant virtual states for the electron-transfer pathway (see Figure 6).

$$H_{ET} = H^{el} + H^h \\ = \frac{H_{el}^* H_{ie}^*}{\Delta E_{(D-S-A)/(D^+S^-A)}} + \frac{H_{ih}^* H'_{fh}}{\Delta E_{(D-S-A)/(D^+S^-A^-)}} \quad (4)$$

$$H_{BET} = \frac{H_{fh} H_{ih}}{\Delta E_{(D^+S^-A^-)/(D^+S^-A)}} \quad (5)$$

In eqs 4 and 5,  $H_{ih}$  and  $H_{fh}$  are the couplings between initial and virtual states and between virtual and final states, respectively, related to the virtual transitions involved in hole-transfer pathways.  $H_{ie}$  and  $H_{fe}$  are the corresponding couplings for the electron-transfer pathways (the asterisk indicates that an excited state plays the role of the initial state; the "prime" symbol on the H indicates that the involved virtual state is also formally an excited state). The  $\Delta E$  values are the energy gaps between the relevant states (explicitly reported as subscripts). It must be noted that the state  $D^+S^-A^-$  is a suitable virtual state for the back electron transfer, but it cannot be used for the forward process since it cannot be obtained from the excited state  $*D-S-A$  by a single electron transfer. Also, for **1–3**, photoinduced oxidative electron transfer is expected to essentially take place by the electron-transfer pathway, using  $D^+S^-A$  as the virtual state (i.e.; in eq 4 the first term dominates).

Also considering the rough approximations used in estimating the energies of the various states schematized in Figure 6, and keeping the discussion at a very qualitative level, it appears that for **2**, the energy gaps between initial and virtual states are significantly larger for the forward than for the back electron transfer. For example, the energy gap between  $*D-S-A$  and  $D^+S^-A$  states (affecting the electron-transfer pathway for forward electron transfer) is approximated to 1.86 eV, whereas the energy gap between  $D^+S^-A^-$  and  $D^+S^-A$  states (affecting the back electron transfer) is approximated to 0.68 eV. On making the reasonable assumption that the matrix elements for the individual steps of the superexchange mechanism (i.e.;  $H_{ie}$ ,  $H_{ih}$ , etc.) are of similar magnitude, these considerations lead to the conclusion that the electronic coupling for the charge recombination process in **2** (as well as in **1** and **3**) is significantly higher than for the charge separation process, and as a consequence the rate constant for charge recombination can well exceed the rate constant for charge separation, even in the presence of less favorable thermodynamics, as indicated by our experimental results on **1–3**.

Some general *qualitative* considerations can be derived from the above discussion. In particular for oxidative photoinduced electron transfer, the hole-transfer pathway can effectively be used for back electron transfer, whereas it is less efficient for the forward process. Because forward and back electron transfer can take advantage of different routes, it is not easy to predict a priori which process is the faster in specific cases; however, a hole-transfer virtual state is available for charge recombination in photoinduced oxidative electron transfer, and the charge recombination process can become faster than charge separation when the spacer is easily oxidizable. This is clearly the case for **1–3**, which contain spacers like biphenylene subunits.

To verify the above statements, we prepared a D-S-A species similar to **2**, but having a single phenylene spacer between the Os(II)-based chromophore and the *head-to-tail*-bipyridinium acceptor: compound **4**, whose molecular structure is shown in Figure 7. The absorption spectrum of **4** (see Figure 7) closely

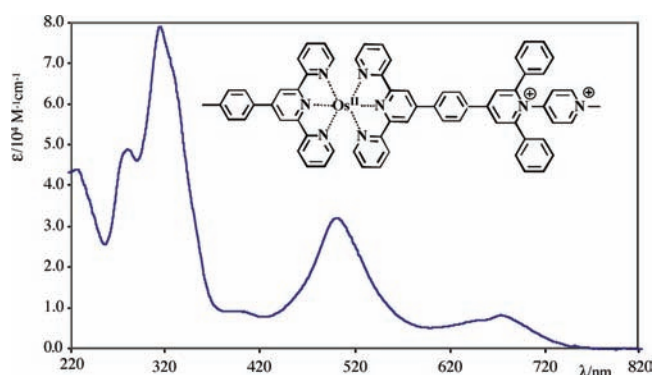


**Figure 7.** Structural formula of **4** (total charge omitted) and its absorption spectrum in MeCN.

resembles those of **1–3** in the visible region; however, the maximum of the singlet MLCT band is red-shifted by about 5 nm, suggesting a slightly increased intercomponent interaction between the metal-based subunit and the bipyridinium acceptor. The main difference between the spectral features of **2** and **4** lies in the UV region, as expected since the absorption band at about 390 nm, attributed to a CT from the biphenylene unit to the acceptor A subunit, is not present in **4**.

Compound **4** displays the classical MLCT phosphorescence at 77 K in rigid matrix, with properties which are very close to those of **D** and **1–3** ( $\lambda_{\text{max}} = 725 \text{ nm}$ ,  $\tau = 2.5 \mu\text{s}$ ), indicating that the shorter phenylene spacer is anyway sufficient to avoid strong mutual perturbation between the donor and acceptor subunits. The MLCT emission is totally quenched at room temperature in MeCN solution, so indicating, as expected, the occurring of an efficient oxidative photoinduced electron transfer from the  $^3\text{MLCT}$  emissive level to the bipyridinium subunit. The energetics of the photoinduced electron transfer processes are not significantly different from that of **2**: the reduction potential (A-centered) of **4** is  $-0.53 \text{ V}$  vs SCE (to be compared with  $-0.58 \text{ V}$  for **2**, see Table 1), and the oxidation potential (Os-based) is  $+0.91 \text{ V}$ , close to that of **2**. Any significant difference in electron transfer rate constants will therefore be related to the nature of the spacer. The presence of a different spacer will influence the electronic coupling for electron transfer  $H_{\text{ET}}$ , but the FCWD factor will also change because the shorter distance between donor and acceptor will modify the reorganization energy of the process. However, we are not seeking to isolate the effect of the spacer on  $H_{\text{ET}}$ , but rather to verify if the absence of a good electron donor spacer can slow down charge recombination *relative* to charge separation.

The transient absorption spectra of **4** at different time delays are shown in Figure 8. The initial transient spectrum, recorded

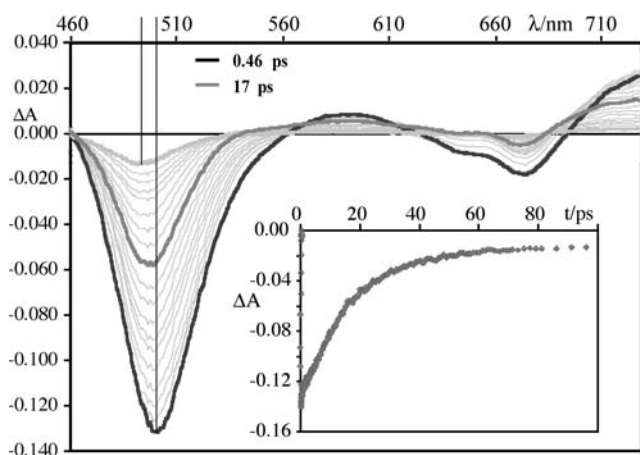
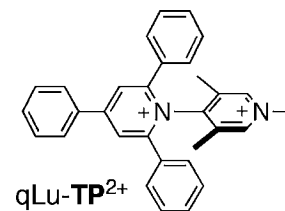


**Figure 8.** Transient absorption spectra of **4**. Time-resolved recovery trace at 500 nm (biexponential, see text) is shown in the inset. The vertical lines are used to evidence the blue-shift with time of the bleaching of the MLCT band.

after 1 ps, is similar to those of the other D-S-A systems studied herein, showing the typical bleedings of the spin-allowed and spin-forbidden MLCT bands, partially balanced at wavelengths longer than 560 nm by contribution of the transient absorption of the reduced terpyridine ligand (which anyway appears to be slightly red-shifted compared to the transient spectra of **1–3**, suggesting a non-negligible influence of the charged bipyridinium unit, only separated from the terpyridine ligand by a single phenylene spacer). However, unlike the transient spectra of the other D-S-A species, the initial spectrum of **4** evolves within about 20 ps to a spectrum which is still similar, but exhibits significant differences: one important difference is that the bleaching at about 500 nm clearly shifts to the blue. This spectral change suggests that a new transient is formed, with blue-shifted absorption compared to initial transient absorption.

The monoreduced form of 1',3',5'-trimethyl-2,4,6-triphenyl-1,4'-bipyridine-1,1'-diium ( $\text{qLu-TP}^{2+}$ , see Chart 2 for the molecular

**Chart 2.** Structural Formula of Compound  $\text{qLu-TP}^{2+}$ , Used as Model for Obtaining Spectral Information on the One-Electron Reduced Bipyridinium Subunit in **4** (See Text)



structure), a bonafide model for the one-electron reduced bipyridinium subunit in **4**, exhibits an absorption band peaking at 530 nm,<sup>28</sup> blue-shifted compared to the absorption of reduced terpyridine, so it can be suggested that the spectral evolution shown in Figure 8 is due to formation of a species where the bipyridinium unit is singly reduced.

The spectral change discussed above is affiliated to the faster component of the biexponential kinetic trace of the bleaching recovery at 500 nm, and takes place in about 10 ps. It is interesting to note that the transient spectra of **4** can be resolved into two time regimes: the transient spectra in first time regime (Figure 9, top panel) exhibit isosbestic points at 563, 641, and 690 nm, with  $\Delta A \neq 0$ . This indicates that two states are essentially involved in the decay process, but the final state is not the ground state. A transient whose absorption is blue-shifted compared to the initial transient absorption is clearly forming. The transient spectra in the second time

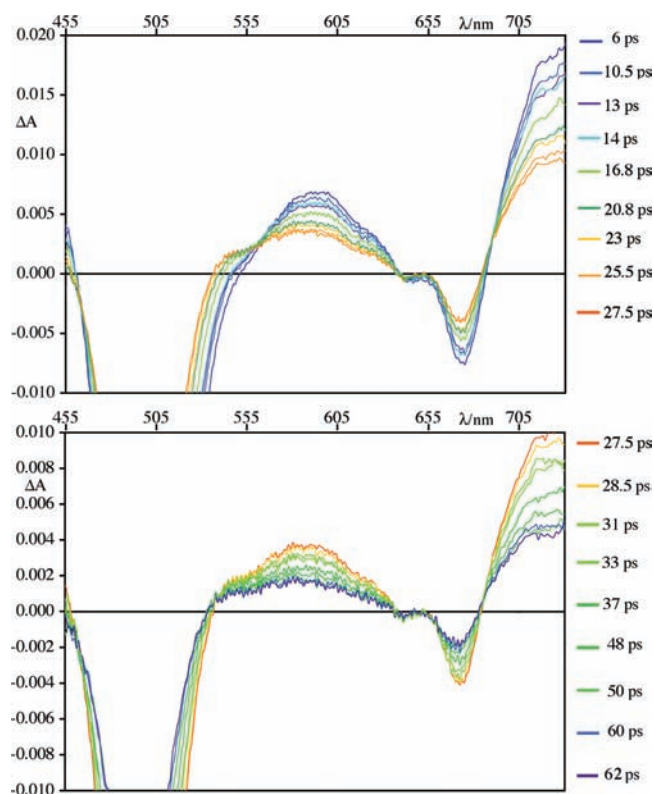


**Figure 9.** Transient spectra of **4**, separated into two different time regimes (see text).

regime (Figure 9, bottom panel) show different isosbestic points at 537, 638, and 684 nm, with  $\Delta A$  close to 0. So it can be concluded that the process occurring during the second time regime, which takes place in about 30 ps, leads to the ground state. We suggest that the faster process is the electron transfer from the reduced terpyridine which is present in the MLCT triplet state to the bipyridinium unit, that is, to formation of the  $D^+ \cdot S-A^-$  charge-separated state from the initially prepared  $^*D-S-A$  state. The circumstance that the spin-allowed and spin-forbidden MLCT bleachings are still present in the new formed state agrees with this assignment.<sup>29</sup>

The global fitting of the transient absorption data, shown in Figure 10, allows to assign the various components of the

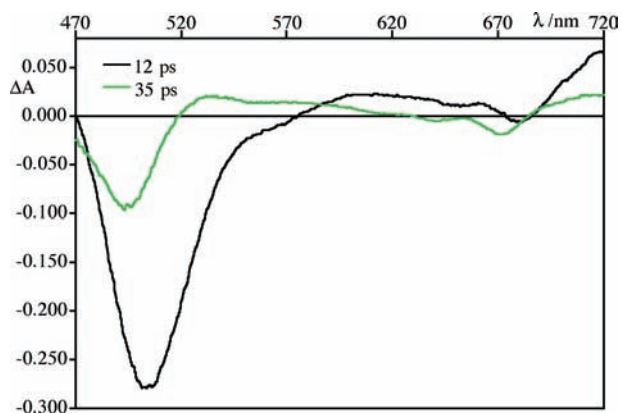


**Figure 10.** Main transient spectra obtained by global fitting of the data shown in Figure 8. The time decays of each component are reported in the figure.

transient spectra to individual states, and helps to further clarify the situation. Actually, the global fitting of the transient data of **4** yields two main components:<sup>30</sup> the shorter-lived component (lifetime, 12 ps) is associated to a transient spectrum roughly identical in shape to those of **1–3** and is so assigned to the MLCT triplet. The longer-lived component (35 ps) is associated to a transient spectrum where the MLCT bleachings are still present but the transient absorption is clearly blue-shifted, indicating the presence of the reduced bipyridinium unit,<sup>28</sup> and is therefore assigned to the charge-separated state.

The results indicate that, while the photoinduced oxidative electron transfer in **4** (rate constant about  $1 \times 10^{11} \text{ s}^{-1}$ ) is clearly accelerated compared to **2** (see Table 3), as expected because of a shorter spacer, the charge recombination is not accelerated to the same extent, allowing accumulation of the charge-separated state. This finding strongly supports our hypothesis that the presence of a spacer with an electron-donating character speeds up charge recombination over charge separation in **1–3**, so hindering the preparation of long-lived charge-separated states, in spite of the apparently favorable thermodynamics.

### 3. CONCLUSIONS

A series of linearly arranged donor-spacer-acceptor (D-S-A) systems, **1–3**, containing an Os(II) polypyridine unit as chromophore, various biphenylene spacers, and (bi)pyridinium acceptors, have been prepared and their absorption spectra, redox behavior, and photophysical properties investigated by combining theoretical and experimental approaches. Also, the model species **D** and a fourth D-S-A system, **4**, containing a

shorter phenyl spacer instead of a biphenylene spacer, have been studied. The results indicate that fast photoinduced oxidative electron transfer takes place in these D-S-A compounds. However, the charge-separated state does not accumulate in **1–3**, because of the presence of the oxidizable biphenylene spacers, which can efficiently contribute to accelerate charge recombination by the hole-transfer superexchange mechanism, whereas the presence of a single phenyl as spacer in **4** makes charge recombination slower than photoinduced charge separation.

The interpretation of the results is based on factors affecting superexchange mechanism for intercomponent electron transfer and allows to infer some considerations which are proposed to be of general validity. It is suggested that long-lived charge separation by oxidative photoinduced electron transfer in  $^*D-S-A$  systems is hindered when spacers possess high-energy occupied MOs because the latter can facilitate an efficient superexchange-mediated charge recombination via the hole-transfer pathway. Similarly, it could be demonstrated that the reverse is valid for reductive photoinduced electron transfer in D-S- $^*A$  systems: in this case, low-energy unoccupied MOs centered on the spacer can limit the possibility of gaining long-lived charge separation because of the intervening of a superexchange-mediated charge recombination via the electron-transfer pathway, which is not efficient for the charge separation process.

It could be noted that the above information is sparingly present in the literature,<sup>14,27,31</sup> but is sometimes buried within other effects. Here the information is clearly obtained, with combined efforts of experimental and theoretical approaches. It should also be noted that a quite recent paper dealing with Ru(II)-containing dyads reports very similar results, with the same remarks about oligophenylene bridges being better suited for charge separation by reductive, rather than oxidative, photoinduced electron transfer.<sup>26</sup> Such considerations can have intriguing consequences on the smart design of D-S-A systems aimed to obtain long-lived charge-separated states: in brief, spacers with high energy HOMO have to be preferably avoided for D-S-A systems featuring oxidative charge separation, whereas spacers with a low energy LUMO have to be preferably avoided for D-S-A systems featuring reductive charge separation.

## 4. EXPERIMENTAL SECTION

**4.1. Syntheses, Characterization, and General Experimental Details.** Materials, syntheses of organic ligands and related osmium(II) dyads along with full characterizations are provided in the Supporting Information.

**4.2. Electrochemical Measurements.** Electrochemical experiments were carried out with a conventional three-electrode cell and a PC-controlled potentiostat/galvanostat (Princeton Applied Research Inc. model 263A). The working electrode was a platinum electrode from Radiometer-Tacussel (area, 0.0314 cm<sup>2</sup>; diameter, 2.0 mm) mounted in Teflon. Platinum wire was used as the counter-electrode and a saturated calomel electrode (SCE) as the reference. Electrolytic solutions, MeCN (Aldrich, anhydrous, 99.8%) containing 0.1 M tetrabutylammonium hexafluorophosphate (TBAPF<sub>6</sub>, Aldrich, +99%) as supporting electrolyte, were routinely deoxygenated by argon bubbling. All potential values are given versus the SCE. The reported numerical values (Table 1) were corrected by using a dissolved Fc<sup>+</sup>/Fc couple as an internal reference and by setting  $E_{1/2}$  (Fc<sup>+</sup>/Fc) equal to +0.380 V vs SCE in MeCN.<sup>32</sup> Cyclic voltammetry experiments were conducted at a scan rate of 0.1 V s<sup>-1</sup>. Experimental uncertainty on potential values is 10 mV.

**4.3. Absorption Spectra and Photophysical Properties.** UV/vis absorption spectra were taken on a Jasco V-560 spectrophotometer.

For steady-state luminescence measurements, a Jobin Yvon-Spex Fluoromax 2 spectrofluorimeter was used, equipped with a Hamamatsu R3896 photomultiplier. The spectra were corrected for photomultiplier response using a program purchased with the fluorimeter. For the luminescence lifetimes, an Edinburgh OB 900 time-correlated single-photon-counting spectrometer was used. As excitation sources, a Hamamatsu PLP 2 laser diode (59 ps pulse width at 408 nm) and/or the nitrogen discharge (pulse width 2 ns at 337 nm) were employed. Time-resolved transient absorption experiments were performed by using a pump–probe setup based on the Spectra-Physics MAI-TAI Ti:sapphire system as the laser source and the Ultrafast Systems Helios spectrometer as the detector. The pump pulse was generated with a Spectra-Physics 800 FP OPA. The probe pulse was obtained by continuum generation on a sapphire plate (spectral range, 450–800 nm). Effective time resolution of about 200 fs, temporal chirp over the white-light 450–750 nm range of about 150 fs; the temporal window of the optical delay stage was 0–3200 ps. The time-resolved data were analyzed with the Ultrafast Systems Surface Explorer Pro software. Experimental uncertainties on the absorption and photophysical data are as follows: absorption maxima, 2 nm; molar absorption, 15%; luminescence maxima, 4 nm; luminescence lifetimes, 10%; luminescence quantum yields, 20%; transient absorption decay and rise rates, 10%.

**4.4. Computational Methods.** All calculations were performed using the Gaussian.<sup>33</sup> Bulk solvent (here MeCN) effects were always included by the means of the Polarizable Continuum Model<sup>34</sup> as implemented in the Gaussian code.<sup>35</sup> The structure of system **2** was optimized at DFT level using the hybrid PBE0 functional<sup>36</sup> and the LANL2DZ basis (and associated pseudopotential for the Os atom<sup>37</sup>) in absence of constraints. The first 15 vertical electronic transition energies (that is up to 305 nm) were computed using the TD-DFT approach using the range separated CAM-B3LYP functional<sup>38</sup> and the same basis set, always including solvent at PCM level.

## ■ ASSOCIATED CONTENT

### ■ Supporting Information

Complete reference 33. Computational results including optimized geometries of dyads along with their related electronic properties (TD-DFT) and structures (involved frontier MOs). Experimental details for the synthesis and characterization of new compounds and precursors, including <sup>1</sup>H NMR (500 MHz) and <sup>13</sup>C NMR (126 MHz) spectra as well as ESI mass spectra. Luminescence spectra of **D** (77 K and room temperature). Transient absorption spectrum and decay of **D**. Schematization of the energy levels and decay processes involved in the excited state decays of **1** and **2**. This material is available free of charge via the Internet at <http://pubs.acs.org>.

## ■ AUTHOR INFORMATION

### ■ Corresponding Author

\*E-mail: [fpuntoriero@unime.it](mailto:fpuntoriero@unime.it) (F.P.), [campagna@unime.it](mailto:campagna@unime.it) (S.C.), [philippe.laine@univ-paris-diderot.fr](mailto:philippe.laine@univ-paris-diderot.fr) (P.P.L.).

### ■ Notes

The authors declare no competing financial interest.

## ■ ACKNOWLEDGMENTS

Dr. Sophie Griveau, Dr. Fethi Bedioui, and Dr. Valérie Marvaud are acknowledged for stimulating discussions. J.F., G.D., I.C., and P.P.L. are grateful to the French National Agency for Research (ANR) “programme blanc” (NEXUS project: ANR-07-BLAN-0277 and SWITCH project: ANR-2010-BLAN-712) for financial support. S.C. and F.P. thanks the MIUR (PRIN project 2008) and FIRB (Nanosolar project, contract no. RBAP11C58Y) for financial support.

## ■ REFERENCES

- (1) The literature on this topic is too vast to be exhaustively quoted. For a few books and review articles, see: (a) Wasielewski, M. R. *Chem. Rev.* **1992**, *92*, 435. (b) Gust, D.; Moore, T. A.; Moore, A. L. *Acc. Chem. Res.* **1993**, *26*, 198. (c) Paddon-Row, M. N. *Acc. Chem. Res.* **1994**, *27*, 18. (d) Newton, M. D. *Chem. Rev.* **1991**, *91*, 767. (e) Closs, G. L.; Miller, J. D. *Science* **1988**, *240*, 440. (f) Balzani, V. *Pure Appl. Chem.* **1990**, *62*, 1099. (g) Meyer, T. J. *Acc. Chem. Res.* **1989**, *22*, 163. (h) Onuchic, J. J.; Beratan, D. N.; Winkler, J. R.; Gray, H. B. *Annu. Rev. Biophys. Biomol. Struct.* **1992**, *21*, 349. (i) Verhoeven, J. W. *Adv. Chem. Phys.* **1999**, *106*, 603. (j) Barbara, P. F.; Meyer, T. J.; Ratner, M. A. *J. Phys. Chem.* **1996**, *100*, 13148. (k) Gray, H. B.; Winkler, J. R. *Annu. Rev. Biochem.* **1996**, *65*, 537. (l) Benniston, A. C.; Harriman, A. *Chem. Soc. Rev.* **2006**, *35*, 169. (m) Gust, D.; Moore, A. L.; Moore, T. A. *Acc. Chem. Res.* **2001**, *34*, 40. (n) *Electron Transfer in Chemistry*; Balzani, V., Ed.; Wiley-VCH: Weinheim, Germany, 2001; Vols. 1–5. (o) Baranoff, E.; Collin, J.-P.; Flamigni, L.; Sauvage, J.-P. *Chem. Soc. Rev.* **2004**, *33*, 147. (p) Lomoth, R.; Magnuson, A.; Sjödin, M.; Huang, P.; Styring, S.; Hammarström, L. *Photosynth. Res.* **2006**, *87*, 25. (q) Albinsson, B.; Martensson, J. J. *Photochem. Photobiol. C: Photochem. Rev.* **2008**, *9*, 138.
- (2) See, for example: (a) Balzani, V.; Credi, A.; Venturi, M. *ChemSusChem* **2008**, *1*, 26. (b) Alstrum-Acevedo, J. H.; Brennaman, M. K.; Meyer, T. J. *Inorg. Chem.* **2005**, *44*, 6802. (c) Reece, S. Y.; Hodgkiss, J. M.; Stubbe, J. A.; Nocera, D. G. *Phil. Trans. R. Soc. B* **2006**, *361*, 1351. (d) Fukuzumi, S. *Bull. Chem. Soc. Jpn.* **2006**, *79*, 177. (e) Rodriguez-Morgade, M. S.; Torres, T.; Atienza-Castellanos, C.; Guldi, D. M. *J. Am. Chem. Soc.* **2006**, *128*, 15145. (f) Grätzel, M. *Acc. Chem. Res.* **2009**, *42*, 1788. (g) Youngblood, W. J.; Lee, S.-H. A.; Maeda, K.; Mallouk, T. E. *Acc. Chem. Res.* **2009**, *42*, 1966. (h) Indelli, M. T.; Chiorboli, C.; Flamigni, L.; De Cola, L.; Scandola, F. *Inorg. Chem.* **2007**, *46*, 5630. (i) De Silva, A. P. *J. Phys. Chem. Lett.* **2011**, *2*, 2865. (j) Song, W.; Chen, Z.; Brennaman, M. K.; Conception, J. J.; Patrocínio, A. O. T.; Murakami Ika, N. Y.; Meyer, T. J. *Pure Appl. Chem.* **2011**, *83*, 749.
- (3) Paddon-Row, M. N. In *Electron Transfer in Chemistry*; Balzani, V., Ed.; Wiley-VCH: Weinheim, Germany, 2001; Vol. 3, p 179.
- (4) Scandola, F.; Chiorboli, C.; Indelli, M. T.; Rampi, M. A. In *Electron Transfer in Chemistry*; Balzani, V., Ed.; Wiley-VCH: Weinheim, Germany, 2001; Vol. 3, p 337.
- (5) (a) Fortage, J.; Tuyères, F.; Ochsenbein, P.; Puntoriero, F.; Nastasi, F.; Campagna, S.; Griveau, S.; Bedioui, F.; Ciofini, I.; Lainé, P. *P. Chem.—Eur. J.* **2010**, *16*, 11047. (b) Peltier, C.; Adamo, C.; Lainé, P. P.; Campagna, S.; Puntoriero, F.; Ciofini, I. *J. Phys. Chem. A* **2010**, *114*, 8434.
- (6) Fortage, J.; Peltier, C.; Nastasi, F.; Puntoriero, F.; Tuyères, F.; Griveau, S.; Bedioui, F.; Adamo, C.; Ciofini, I.; Campagna, S.; Lainé, P. *J. Am. Chem. Soc.* **2010**, *132*, 16700.
- (7) (a) Lainé, P. P.; Bedioui, F.; Loiseau, F.; Chiorboli, C.; Campagna, S. *J. Am. Chem. Soc.* **2006**, *128*, 7510. (b) Lainé, P. P.; Campagna, S.; Loiseau, F. *Coord. Chem. Rev.* **2008**, *252*, 2552.
- (8) Balzani, V.; Scandola, F. *Supramolecular Photochemistry*; Horwood: Chichester, U.K., 1991.
- (9) Vlček, A.; Zláliš, S. *Coord. Chem. Rev.* **2007**, *251*, 258.
- (10) (a) Lainé, P. P.; Loiseau, F.; Campagna, S.; Ciofini, I.; Adamo, C. *Inorg. Chem.* **2006**, *45*, 5538. (b) Lainé, P. P.; Ciofini, I.; Ochsenbein, P.; Amouyal, E.; Adamo, C.; Bedioui, F. *Chem.—Eur. J.* **2005**, *11*, 3711. (c) Ciofini, I.; Lainé, P. P.; Bedioui, F.; Adamo, C. *J. Am. Chem. Soc.* **2004**, *126*, 10763.
- (11) Jacquemin, D.; Perpète, E.; Ciofini, I.; Adamo, C. *Acc. Chem. Res.* **2009**, *42*, 326.
- (12) It is worth noting that in the present work only spin-allowed excitations (i.e., singlet-to-singlet transitions) were computed by the means of TD-DFT. As regards forbidden singlet-to-triplet excitations, experimentally observed due to the large spin–orbit coupling of osmium(II) (heavy-atom effect), they were assessed using a DSCF approach.<sup>13</sup> The lowest-lying singlet-to-triplet transition was computed at the CAM-B3LYP level to occur at 703 nm, in good agreement with the experimental band observed at ca. 676 nm.

(13) The singlet-to-triplet transition energy is estimated as difference in total energy between the singlet and the triplet.

(14) Comparison between computed and experimental absorption data also reveals some interesting information: (i) as the experimental absorption spectra of **D** and **1–3** are very close (see Figure 2) in the MLCT region, evidently the contribution of the (H-1)-(L+2) transition (which according to the calculation contributes by about 20% to the computed oscillator strength) to the computed 459 nm band does not significantly modify the experimental spectrum; (ii) the computed energies of the CT bands involving metal-based orbitals are overestimated with respect to the experimental values whereas the computed energies of the CT bands essentially involving organic moieties (that is, the S and A subunits) are much closer to the experimental values. Nevertheless, the error associated to the MLCT transition (0.2 eV) is still in the range of accuracy expected at this level of theory, and the better results obtained for transitions centered on the organic subsystems can be ascribed both to their short-range CT character and to the fact that they do not involve metal orbitals.

(15) Kumaresa, D.; Shankar, K.; Vaidya, S.; Schmehl, R. H. *Top. Curr. Chem.* **2007**, *281*, 101, and refs therein..

(16) The work term  $W$  is neglected here in a first approximation for the calculation of  $\Delta G^0$ . Even though  $W$  is not insignificant in the present case because of the modest value of the driving force, this approximation does not alter the discussion.

(17) (a) Amoroso, A. J.; Das, A.; McCleverty, J. A.; Ward, M. D.; Barigelletti, F.; Flamigni, L. *Inorg. Chim. Acta* **1994**, *226*, 171. (b) Gaines, G. L.; O'Neil, M. P.; Svec, W. A.; Niemczyk, M. P.; Wasielewski, M. R. *J. Am. Chem. Soc.* **1991**, *113*, 719. (c) Chen, P.; Meyer, T. J. *Chem. Rev.* **1998**, *98*, 1439, and refs therein.

(18) (a) Ford, W. E.; Rodgers, M. A. J. *J. Phys. Chem.* **1992**, *96*, 2917. (b) Tyson, D. S.; Luman, C. R.; Zhou, X.; Castellano, F. N. *Inorg. Chem.* **2001**, *40*, 4063. (c) McClenaghan, N. D.; Barigelletti, F.; Maubert, B.; Campagna, S. *Chem. Commun.* **2002**, 603. (d) Passalacqua, R.; Loiseau, F.; Campagna, S.; Fang, Y.-Q.; Hanan, G. S. *Angew. Chem., Int. Ed.* **2003**, *42*, 1608. (e) Wang, X. Y.; Del Guerso, A.; Schmehl, R. H. *J. Photochem. Photobiol. C: Photochem. Rev.* **2004**, *5*, 55. (f) McClenaghan, N. D.; Maubert, B.; Indelli, M. T.; Campagna, S. *Coord. Chem. Rev.* **2005**, *249*, 1336.

(19) Maubert, B.; McClenaghan, N. D.; Indelli, M. T.; Campagna, S. *J. Phys. Chem. A* **2003**, *107*, 447.

(20) (a) McConnell, H. M. *J. Chem. Phys.* **1961**, *35*, 508. (b) Jordan, K. D.; Paddon-Row, M. N. *Chem. Rev.* **1992**, *92*, 395. (c) Reimers, J. R.; Hush, N. S. *J. Photochem. Photobiol. A: Chem.* **1994**, *82*, 31.

(21) Note that forward electron transfer in **1** is slower than the equilibration rate constant, whose value is the sum of forward and back electron transfer between the MLCT and the charge-separated state.

(22) For initially formed transient absorption spectra, here we mean the spectra obtained after 5 ps from laser pulse, so ultrafast processes such as vibrational cooling and intersystem crossing, which in Os(II) polypyridine complexes are known to be faster,<sup>23</sup> are not taken into consideration.

(23) (a) Andersson, J.; Puntoriero, F.; Serroni, S.; Yartsev, A.; Pascher, T.; Polivka, T.; Campagna, S.; Sundström, V. *Chem. Phys. Lett.* **2004**, *386*, 336. (b) Andersson, J.; Puntoriero, F.; Serroni, S.; Yartsev, A.; Pascher, T.; Polivka, T.; Campagna, S.; Sundström, V. *Faraday Discuss.* **2004**, *127*, 295.

(24) These values are the energies of the charge-separated states, estimated by subtracting the driving force of the photoinduced electron transfer, calculated by eq 1 (Table 3) from the energy of the <sup>3</sup>MLCT states (1.72 eV, identical for all compounds).

(25) The energy gap between the initial state and the virtual state should be calculated at the nuclear coordination geometry of the surfaces' avoided crossing, where initial and final states have the same energy. So, the energy gap values  $\Delta E$  present in eqs 4 and 5 are not exactly the ones calculated in this work. However, they are considered good enough for our (qualitative) discussion.

(26) Indelli, M. T.; Orlandi, M.; Chiorboli, C.; Ravaglia, M.; Scandola, F.; Lafolet, F.; Welter, S.; De Cola, L. *J. Phys. Chem. A* **2012**, *116*, 119.

(27) Grzeszczuk, M.; Smith, D. E. *J. Electroanal. Chem.* **1983**, *157*, 205.

(28) Fortage, J.; Peltier, C.; Perruchot, C.; Takemoto, Y.; Teki, Y.; Bedioui, F.; Marvaud, V.; Dupeyre, G.; Pospisil, L.; Adamo, C.; Hromadova, M.; Ciofini, L.; Lainé, P. P. *J. Am. Chem. Soc.* **2012**, *134*, 2691.

(29) In  $[\text{Os}(\text{phtpy})_2]^{2+}$  and related dyads, a fast process is also known to occur within few ps. This process, not explored in the systems here investigated, is planarization of the phenyl connected to the terpy ligand. So one could ask if the process assigned to forward electron transfer in **2** cannot simply be planarization. However, planarization has the effect of slightly modifying the reduced terpy transient absorption and manifests itself by a change in the transient absorption at wavelengths longer than 680 nm,<sup>7a</sup> and it cannot be the cause for the spectral changes in the 450–550 nm region.

(30) For convergence, the fitting requires the presence of another component with lifetime of <2 ps. This component could cumulate various ultrafast processes,<sup>7</sup> leading to the thermally equilibrated triplet MLCT state. These processes are not investigated here.

(31) See for example: (a) Weiss, E. A.; Ahrens, M. J.; Sinks, L. E.; Gusev, A. V.; Ratner, M. A.; Wasielewski, M. R. *J. Am. Chem. Soc.* **2004**, *126*, 5577. (b) Walther, M. E.; Wenger, O. S. *ChemPhysChem* **2009**, *10*, 1203.

(32) Pavlishchuk, V. V.; Addison, A. W. *Inorg. Chim. Acta* **2000**, *298*, 97.

(33) Frisch, M. J. et al. *Gaussian 09*, Revision A.02; Gaussian Inc.: Wallingford, CT, 2009.

(34) Tomasi, J.; Mennucci, B.; Cammi, R. *Chem. Rev.* **2005**, *105*, 2999.

(35) Barone, V.; Cossi, M. *J. Phys. Chem. A* **1998**, *102*, 1995.

(36) Adamo, C.; Barone, V. *J. Chem. Phys.* **1999**, *110*, 6158.

(37) (a) Dunning, T. H., Jr.; Hay, P. J. In *Modern Theoretical Chemistry*; Schaefer, H. F., III, Ed.; Plenum: New York, 1976; Vol. 3, p 1. (b) Hay, P. J.; Wadt, W. R. *J. Chem. Phys.* **1985**, *82*, 299.

(38) Yanai, T.; Tew, D.; Handy, N. *Chem. Phys. Lett.* **2004**, *393*, 51.